RSC Advances

ROYAL SOCIETY OF CHEMISTRY

www.rsc.org/advances

Cite this: DOI: 10.1039/c0xx00000x

www.rsc.org/xxxxxx

ARTICLE TYPE

Three 3D Coordination Polymers Based on [1,1':4',1''-terphenyl]-2',4,4'',5'-tetracarboxylate Demonstrating Magnetic Properties and Selective Sensing Al^{3+}/Fe^{3+}over Mixed Ions

Bei-Bei Kang, Na Wei and Zheng-Bo Han*

Received (in XXX, XXX) Xth XXXXXXXXX 20XX, Accepted Xth XXXXXXXXX 20XX
DOI: 10.1039/b000000x

Three three-dimensional (3D) coordination polymers with the formula, $[Cd(TPTC)_{0.5}(H_2O)_2]\cdot DMA$ (**1**), $[Co_2(TPTC)(H_2O)_{1.5}(CH_3OH)_{0.5}]$ (**2**) and $[Mn_2(TPTC)(H_2O)(DMA)]\cdot DMA$ (**3**) (TPTC = [1,1':4',1''-terphenyl]-2',4,4'',5'- tetracarboxylate acid), have been solvothermally synthesized and characterized by thermogravimetric analyses, IR spectroscopy, X-ray powder diffraction and single crystal X-ray diffraction. **1** features a 3D porous coordination polymer constructed by Cd-carboxylate chains and the TPTC bridges. In **2** and **3,** the uniform metal-carboxylate chains with the triple bridges (μ-EO-H_2O)(μ-*syn,syn*-$COO)_2$ and (μ-EO-H_2O/DMA)(μ-*syn,syn*-$COO)_2$ (EO = end-on) are extended by the TPTC arms. Complex **1** displays strong fluorescent emission in the visible region, interestingly, the emission intensities of **1** enhanced upon the addition of Al^{3+} and quenched upon the additional Fe^{3+} over mixed ions. **1** can act as useful material for the sensing of Fe^{3+} and Al^{3+} ions. The magnetic studies of **2** and **3** show that there exist antiferromagnetic interactions between the Co(II) and Mn(II) centers.

Introduction

Nowadays, metal-organic coordination polymers or metal organic frameworks (MOFs) have been becoming a more and more promising area, for their artistically crystalline structure as well as their enormous practical applications, such as gas adsorption and separation,[1] catalysis,[2] luminescence,[3] electrical conductivity,[4] magnetism.[5] It should be noted that a number of luminescent materials sensing to small molecules or metal ions are widely exploited in many areas, such as luminescent probes in biomedical assays and time-resolved microscopy, fluorescent lighting, luminescent probes for chemical species,[6] which have made the MOFs chemosenors reach hotspots.[7] MOFs offer high photoluminescence efficiency, based on components, antennae effects, adsorbate-based emission and sensitization, surface functionalization, and so on.[8] Recently, studies on luminescent MOFs for sensing metal ions have been developed significantly, and some successful fluorescent probes have been employed to determine the concentration of metal ions, such as Ca^{2+}, Cd^{2+} and Fe^{3+}.[9]

The design and construction of functional porous MOFs with magnetic properties, is a challenge because it is difficult to obtain simultaneously large pore sizes and relatively strong magnetic interactions.[10] Magnetic superexchange requires relatively short exchange pathways between two adjacent metal centers. The most popular synthetic strategy is using magnetic chains or clusters connected by longer organic linkers to form a porous open framework.[11]

Organic carboxylate ligands have been widely used in synthesizing MOFs with esthetical structures and unusual properties because of the controllable length of ligand and the various coordination modes of the carboxyl group.[12] Herein, we chose a new quadrangular ligand, namely H_4TPTC, [1,1':4',1''-terphenyl]-2',4,4'',5'-tetracarboxylic acid. Herein, we present a study of three 3D porous MOFs, $[Cd(TPTC)_{0.5}(H_2O)_2]\cdot DMA$ (**1**), $[Co_2(TPTC)(H_2O)_{1.5}(CH_3OH)_{0.5}]$ (**2**) and $[Mn_2(TPTC)(H_2O)(DMA)]\cdot DMA$ (**3**), which were generated by changing only the metal salt. More interestingly, **1** exhibits Al^{3+}/Fe^{3+}-modulated fluorescence over mixed ions; **2** and **3** also show antiferromagnetic interactions between metal ions.

Experimental Section

Materials and Methods

All chemicals were commercially available and used without further purification. The C, H, and N microanalyses were carried out with Perkin-Elmer 240 elemental analyzer. The FT-IR spectra were recorded from KBr pellets in the 4000-400 cm^{-1} range on a Nicolet 5DX spectrometer. Thermogravimetric analyses (TGA) were taken on a Perkin-Elmer Pyrisl (20-800 ^oC, 10 ^oC min^{-1}, flowing N_2(g)). X-ray powder diffraction were recorded with a Bruker AXS D8 advanced automated diffractometer with Cu-Kα radiation. Luminescence spectra for the solid samples and liquid samples were investigated with a Hitachi F-4500 fluorescence spectrophotometer and Varian Cary Eclipse Fluorescence spectrophotometer, respectively. The magnetic data were collected on a Quantum Design MPMS SQUID-XL-5 magnetometer.

Solvothermal synthesis

Table 1 Crystallographic Data for **1-3**.

	1	**2**	**3**
Empirical formula	$C_{15}H_{18}CdNO_7$	$C_{22.5}H_{15}Co_2O_{10}$	$C_{30}H_{28}Mn_2N_2O_{11}$
Formula weight	436.70	563.21	702.42
Wavelength/ Å	0.71073	0.71073	0.71073
Crystal system	Monoclinic	Monoclinic	Monoclinic
Space group	$P2_1/c$	$C2/m$	$P2_1/n$
a/ Å	8.7173(6)	18.7009(15)	12.6852(11)
b/ Å	19.4288(17)	7.2352(5)	14.7613(15)
c/ Å	9.6558(8)	12.5595(9)	16.0030(15)
β/ °	97.170(3)	123.488(2)	98.210(3)
V/ Å^3	1622.6(2)	1417.27(18)	2965.9(5)
Z	4	2	4
Dc/mg m^{-3}	1.788	1.320	1.573
μ/ mm^{-1}	1.383	1.215	0.917
F(000)	876	568	1440
Range for data collection/°	2.99-25.00	3.10-26.38	3.05-26.38
Reflections collected	2800	5869	17987
Max., min. transmission	0.7694, 0.7064	0.7775, 0.6633	0.8052, 0.7290
T/ K	173(2)	173(2)	173(2)
Data/restraints/parameters	2800 / 24 / 225	1516 / 60 / 116	5467 / 18 / 417
Final R indices [$I > 2\sigma(I)$][a]	R_1 = 0.0479, wR_2 = 0.0782	R_1 = 0.0849, wR_2 = 0.2254	R_1 = 0.0503, wR_2 = 0.0886
R indices (all data)	R_1 = 0.0767, wR_2 = 0.0859	R_1 = 0.1206, wR_2 = 0.2481	R_1 = 0.1394, wR_2 = 0.1136
Largest diff. peak and hole /e Å^{-3}	0.891, -0.860	1.417, -0.951	0.546, -0.442

[a] $R_1 = \sum||F_o|-|F_c||/\sum|F_o|$; $wR_2 = \sum[w(F_o^2-F_c^2)^2]/\sum[w(F_o^2)^2]]^{1/2}$

$[Cd(TPTC)_{0.5}(H_2O)_2]\cdot DMA$ (1). A mixture of $Cd(NO_3)_2\cdot 4H_2O$ (0.049 mmol, 0.015 g), H_4TPTC (0.012 mmol, 0.005 g), N,N′-dimethylacetamide (DMA) (1.5 mL) and H_2O (0.5 mL) was stirred for 20 mins in a 5 mL vial, which was heated in an oven to 75 °C for 72 hours. White block crystals were obtained and washed with distilled water and dried in air (yield: *ca*. 54%). Elemental analysis calcd (%) for **1** $C_{15}H_{18}CdNO_7$ (%): C: 41.25; H: 4.15; N: 3.21; found: C: 42.82; H: 4.49; N: 3.41. IR (KBr, cm^{-1}): 3306s, 2922w, 1590vs, 1385vs, 1258m, 1183m, 1016 m, 871 m, 783m.

$[Co_2(TPTC)(H_2O)_{1.5}(CH_3OH)_{0.5}]$ **(2).** The synthesis of **2** was similar to that of **1**, except $Cd(NO_3)_2\cdot 4H_2O$ was instead of $Co(NO_3)_2\cdot 6H_2O$ (0.052 mmol, 0.015 g) (yield: *ca*. 65%). Elemental analysis calcd (%) for **2** $C_{22.5}H_{15}Co_2O_{10}$ (%): C: 47.98; H: 2.68; found: C: 48.15; H: 2.38. IR (KBr, cm^{-1}): 3563w, 2932w, 1590vs, 1412 vs, 1347m, 1254m, 1152m, 868m, 781m.

$[Mn_2(TPTC)(H_2O)(DMA)]\cdot DMA$ (3). The synthesis of **3** was similar to that of **1**, $Cd(NO_3)_2\cdot 4H_2O$ was instead of $Mn(NO_3)_2\cdot 6H_2O$ (0.052 mmol, 0.015 g) (yield: *ca*. 72%). Elemental analysis calcd (%) for **3** $C_{30}H_{30}Mn_2N_2O_{11}$ (%): C: 51.15; H: 4.29; N: 3.98; found: C: 51.25; H: 4.36; N:3.98. IR (KBr, cm^{-1}): 3548w, 2936w, 1591vs, 1414vs, 1347m, 1255m, 1152m, 867m, 782m.

X-ray Crystallography

Crystallographic data of all the complexes were collected at 173 K with a Apex II diffractometer with Mo-Kα radiation (λ = 0.71073 Å) and graphite monochromator using the ω-scan mode. The structure was solved by direct methods and refined on F^2 by full-matrix least squares using SHELXTL.[13] In **2**, DMA molecules were highly disordered, and attempts to locate and refine the peaks were unsuccessful. The DMA molecules were removed from the data set using the SQUEEZE routine of PLATON[14] and refined further using the data generated. Crystallographic data and experimental details for structural analyses are collected in Table 1. The CCDC reference number 1013700-1013702 for **1-3**.

Chart 1 Structure of H_4TPTC.

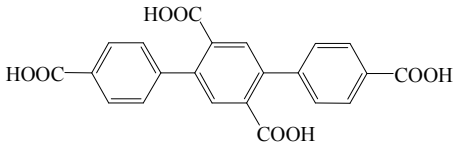

Results and discussion

Crystal Structures

Single-crystal X-ray structure analysis reveals that **1** crystallizes in the monoclinic space group $P2_1/c$, showing a 3D non-interpenetrated framework. The asymmetric unit of **1** contains one crystallographically independent Cd(II) center, a half TPTC ligand, two aqua ligands, and a disordered DMA molecule. As shown in Fig. 1a and 1b, the TPTC ligand coordinate to six Cd(II) ions *via* its four carboxylate groups, two of which adopt chelating mode and the rest two adopt monodentate coordination modes. The central Cd(II) ion is coordinated by four oxygen atoms of TPTC ligands and two aqua ligands. Thus, the central Cd(II) ions are connected by TPTC ligands through their two $\eta^1:\eta^1$ chelating and two *syn-anti*-μ_2-$\eta^1:\eta^1$ carboxylate groups to generate a 2D layer (Fig. 1c), which is further connected by the carboxylate groups of TPTC ligands to form a 3D framework with the channel dimensions of 8.212×7.124 Å^2 (including van der Waals radii of the atoms), and neighboring metal ions are linked by the haploid (*syn-anti*-COO) which induces a 1D uniform Cd-carboxylate chain running along the *a*-axis, with Cd-Cd separation of 4.889 Å (Fig. 1d).

Different from **1,** complex **2** crystallizes in the monoclinic space group $C2/m$. There are half a Co(II) ion, 1/4 fully-deprotonated TPTC ligand, 0.375 μ_2-aqua ligand, and 1/8 CH_3OH molecule in the asymmetric unit of **2**. The CH_3OH molecule maybe come from the impurity of the DMF solvent. As shown in

Fig. 2a and 2b, each TPTC ligand connects eight Co(II) ions and each Co(II) links to four ligands. The coordination geometry around the Co(II) center can be described as a distorted octahedron with the O-Co-O bond angles ranging from 84.9(3) to 180.0(2), and the Co-O bond lengths ranging from 2.051(5) to 2.172(4) Å. The carboxylate groups of TPTC exhibit μ_2-η^1:η^1 bridging fashion and adopt *syn-syn* coordination configuration and neighboring metal ions are linked by the triple (μ-EO-H_2O)(μ-*syn,syn*-$COO)_2$, with Co-Co=3.6176(2) Å, which induces a 1D uniform Co-carboxylate chain running along the *c*-axis (Fig. 2c). The TPTC ligand uses its four carboxylate groups separating the metal ions from different chains by 9.350 Å and 10.751 Å.

The single-crystal X-ray diffraction analysis reveals that complex **3** crystallizes in a monoclinic $P2_1/n$ space group. The asymmetric unit of **3** is composed of three crystallographically independent Mn(II) center, one fully-deprotonated TPTC ligand, one μ_2-aqua ligand, one μ_2-DMA molecule and one free DMA molecule. As shown in Fig. 3a and 3b, the three types of Mn are all six-coordinated with distorted octahedral geometry, with four carboxylate O atoms from four different TPTC ligands, and additionally with two O atoms from one aqua and one terminally coordinated DMA for Mn1, two DMA for Mn2 and two aqua ligands for Mn3, respectively. Similar to **2**, the carboxylate groups of TPTC adopt *syn-syn* coordination configuration and neighboring metal ions are linked by the triple (μ-EO-H_2O/DMA)(μ-*syn,syn*-$COO)_2$. Thus, **3** is built on 1D Mn carboxylate chains and TPTC bridges (Fig. 3c) and further was connected by the TPTC ligands which induces a large 1D irregular quadrangular channel with the dimensions of approximately 9.944×6.286 $Å^2$ (including van der Waals radii of the atoms) (Fig. 3d).

PXRD patterns and thermogravimetric analysis

The simulated and experimental XRD patterns of three compounds are shown in Fig. S1-S3. Their peak positions are in good agreement with each other, confirming the purity of synthesized bulk materials. The TGA curve (Fig. S4) of **1** shows the first weight loss of 12.1% at *ca*. 275 °C, corresponding to the release of free DMA molecules (calcd 19.9%). For complex **2** (Fig. S5), the first weight decrease of 27.0% appears in the range of 163 to 235 °C which is consistent with the loss of coordinated water molecule and two lattice DMA molecules (calcd 26.9%), and the second loss of 52.3% between 360 and 390 °C implies a sudden decomposition which corresponds to the collapse of framework. The TGA curve (Fig. S6) of **3** displays a decrease of 26.16% from 170 to 240 °C, coinciding with the loss of the aqua ligands and DMA molecules (calcd 27.3%), and then the framework collapse upon further heating.

Photoluminescence properties

Previous studies have shown that d^{10} coordination polymers containing zinc may exhibits photoluminescence properties.[15] The luminescent properties of **1** were investigated. As expected, **1** exhibits extraordinary photoluminescence behaviour in the solid state (Fig. S7) and in methanol suspension. In the solid state, strong fluorescent emission band at 387 nm was observed at room temperature, excited at 274 nm, and in methanol solution, the fluorescent emission band at 390 nm was observed at room temperature, excited at 250 nm. It should be noted that **1** shows blue-shifted emission band to different extents with weakened intensities compared with the free H_4TPTC ligand (Fig. S8), which is probably originated from the ligand-to-metal charge transfer (LMCT).[16]

Based on the XRD patterns(Fig. S9), complex **1** retains its framework after immersed in methanol solution containing different metal ions.The effects of a variety of relevant cations K^+, Na^+, Ag^+, Ca^{2+}, Cd^{2+}, Co^{2+}, Cu^{2+}, Hg^{2+}, Ni^{2+}, Zn^{2+}, Al^{3+}, Cr^{3+}, Gd^{3+}, In^{3+} and Fe^{3+} on the fluorescent intensities of **1** were investigated, and the luminescent properties are recorded and shown in Fig. 4. The result indicates that the emission intensity of **1** increased significantly upon addition of Al^{3+} and the emission intensity of **1** almost quenched upon addition of Fe^{3+}. The highest peak at 390 nm is at least twice as intense as the corresponding band in the solution without Al^{3+}. While the introduction of other metal ions caused the intensity to be either unchanged or weakened.

It is well-known that the luminescent intensity of the M^{n+} relies on the efficiency of the energy transfer from the ligand to M^{n+} center.[17] Sun *et al*. prepared $[H_2N(CH_3)_2][Eu(H_2O)_2(BTMIPA)]\cdot 2H_2O$, with $[H_2N(CH_3)_2]^+$ located in the channels, which can be replaced by Fe^{3+} and Al^{3+} and further have a significant effect on the luminescence emissions.[18(a)] As the study of the reported metal-sensitive luminescent metal probes, the change of luminescent intensity in our investigate may result from that the intramolecular energy transfer process is more effective from the TPTC ligand to the Cd(II) with the addition of Al^{3+}, while with the additional Fe^{3+}, this energy transfer process is less effective.

To further explore the fluorescence quenching and enhancement, detailed studies on the luminescence properties of **1** when Fe^{3+} and Al^{3+} ions are present,were carried out. Concentration-dependent luminescence measurements were also carried out (Fig. S10a and b). However, the PL intensities for Fe^{3+}- and Al^{3+}-loaded samples are quite different upon the increase of the concentration. For the Fe^{3+}-loaded sample, the PL intensity decreases gradually, and when the concentration reaches 10^{-3} mol L^{-1}, the luminescence quenches completely. For the Al^{3+}-loaded sample, the PL intensity increases gradually and reaches a maximum at a concentration of 9×10^{-4} mol L^{-1}, and after that, the intensity decreases gradually. On the basis of these results, we report a mechanism: firstly, it is possible for the Fe^{3+} and Al^{3+} ions to bind on the inner surface of the channels. In the structure of **1**, the the carboxylic oxygen atoms inside of the channel, the coordinated water molecules located on Cd^{2+}, and the water molecules in the channel can create a favorable coordination environment for metal ions. Secondly, the exchange between Fe^{3+}/Al^{3+} and Cd^{2+} may result in that the framework of **1** collapsed.[18]

In order to check the high selectivity to Al^{3+} and Fe^{3+} ions over other metal ions, we have studied the luminescence of **1** in a methanol solution containing mixed metal ions (the mixed ions can be Na^+, Hg^{2+}, Mg^{2+}, Ni^{2+}, Zn^{2+}). The emission spectrum of the mixed-ion-loaded methanol solution decreases significantly, compared to the original one, as shown in Fig. 5a. However, when **1** was immersed in a methanol solution containing mixed

metal ions including Fe^{3+} ions, the luminescence of **1** is quenched, indicating that the selectivity for Fe^{3+} ions is not interfered by the existence of other metal ions. The detection of Al^{3+} ions over other metal ions was also carried out and the emission spectrum shows that the intensity decreases significantly when Al^{3+} ions are absent, but the luminescence is enhanced when Al^{3+} ions are present, as shown in Fig. 5b. At low concentration of Al^{3+}/Fe^{3+} in mixed metal ions, **1** can also highly sense Al^{3+}/Fe^{3+} ions (Fig. S10). Thus, **1** can be a good material used for the selective-sensing of Fe^{3+} and Al^{3+} ions. The highly sensing function of **1** indicates the promise of this type of luminescent materials for the sensing ions in biological systems.[19]

Magnetic properties

Magnetic measurements have been applied on crystalline samples of complexes **2** and **3** in the 2-300 K temperature range under 1 kOe, and the χ_M and $\chi_M{}^T$ versus T curves are shown in Fig. 6, respectively. The two compounds are actually 3D porous frameworks, but from the standpoint of magnetism, they can be considered as linear Co-(μ_2-O)-Co and Mn-(μ_2-O)-Mn chains, linked by the long carboxylate bridging ligands.

For complex **2**, the χ_M increases with decreasing temperature, reaching a maximum of 0.04 $cm^3\ mol^{-1}$ at around 2.19 K. The $\chi_M T$ value per two Co(II) unit at 300 K is 2.58 $cm^3\ K\ mol^{-1}$, which is lower than the spin-only value 3.75 $cm^3\ K\ mol^{-1}$ expected for two magnetically isolated Co(II) ions (S = 3/2, g = 2.0).[20] By decreasing the temperature, the $\chi_M T$ gradually decreases by a small amount from 2.58 $cm^3\ K\ mol^{-1}$ at 300 K to *ca*. 80 K, then a little more steeply, reaching 0.76 $cm^3\ K\ mol^{-1}$ at 2.0 K, suggesting a dominant antiferromagnetic interaction between Co(II) centres.[21] The inverse susceptibility plot as a function of temperature is linear above 100 K, following the Curie–Weiss law with a Weiss constant, θ = -42.22 K, and a Curie constant, C = 0.74 $cm^3\ K\ mol^{-1}$, the negative Weiss constant indicating that there exists predominantly antiferromagnetic interaction between two adjacent Co(II) centres. However, there is a jump of the $\chi_M T$ vs. T plot at *ca*. 250 K that cannot be explained by the current model. This cannot be caused from a structural transition as the crystal of **2** remains unchanged down to 100K. Other effect beyond a structural transformation has not yet been found.[22]

For complex **3**, the χ_M increases with decreasing temperature, reaching a maximum of 0.02 $cm^3\ mol^{-1}$ at around 2.09 K. The $\chi_M T$ value per Mn(II) unit at 300 K is 6.72 $cm^3\ K\ mol^{-1}$, which is much lower than the spin-only value 13.12 $cm^3\ K\ mol^{-1}$ expected for three magnetically isolated Mn(II) ions (S = 5/2, g= 2.0). By decreasing the temperature, the $\chi_M T$ gradually decreases by a small amount from 6.72 $cm^3\ K\ mol^{-1}$ at 300 K to *ca*. 80 K, then a little more steeply, reaching 0.43 $cm^3\ K\ mol^{-1}$ at 2.0 K, suggesting a diamagnetic ground state between Mn(II) centres.[23] The inverse susceptibility plot as a function of temperature is linear above 100 K, following the Curie-Weiss law with a Weiss constant, θ = -7.32 K, and a Curie constant, C = 0.23 $cm^3\ K\ mol^{-1}$, the negative Weiss constant indicating that there exists predominantly antiferromagnetic interaction between two adjacent Mn(II) centres.

Conclusions

In summary, three 3D coordination polymers have been successfully constructed from the rigid quadrangular ligand and different metal ions under the same reaction condition. **1-3** exhibit different structures based on metal-carboxylate chains incorporating the TPTC ligand bring these materials excellent properties. **1** exhibits strong luminescence emission in the solid state and in methanol suspension at room temperature. And the luminescence of **1** displayed high performance selectivity for Al^{3+} and Fe^{3+}, which implies that it may be used as luminescent probes of Al^{3+} or Fe^{3+}. The magnetic studies of **2** and **3** showed that there exist antiferromagnetic interactions between the metal centers.

Acknowledgment

This work was granted financial support from National Natural Science Foundation of China (Grant 20871063, 21271096), Liaoning BaiQian Wan Talents (2010921066), the Program for Liaoning Excellent Talents in University (LR2011001), the Liaoning Natural Science Foundation, China (201102079), the Innovative Team Project of Department of Education of Liaoning Province, China (LT2011001), and the Liaoning University 211-Projects of the third period.

Supporting Information Available: The TGA curves, simulated, experimental X-ray powder diffraction patterns and X-ray crystallographic file (CIF) for **1-3**.

References

1. (a) O. M. Yaghi, M. O'Keeffe, N. W. Ockwig, H. K. Chae, M. Eddaoudi, *J. Nature,* 2003, **423**, 705; (b) J.-P. Zhang, Y.-B. Zhang, J.-B. Lin, X.-M. Chen, *Chem. Rev*., 2012, **112**, 1001; (c) J.-R. Li, R. J. Kuppler, H.-C Zhou, *Chem. Soc. Rev*., 2009, **38**, 1477.
2. (a) S. K. Ghosh, J. P. Zhang, S. Kitagawa, *Angew. Chem*., *Int. Ed*., 2007, **46**, 7965; (b) S. K. Ghosh, S. Bureekaew, S. Kitagawa, *Angew. Chem*., *Int. Ed*., 2008, **47**, 3403; (c) L. Ma, C. Abney, W. Lin, *Chem. Soc. Rev.,* 2009, **38**, 1248.
3. (a) Y. Cui, Y. Yue, G. Qian, B. Chen, *Chem. Rev*., 2012, **112**, 1126; (b) C. Wang, O. Volotskova, K. Lu, M. Ahmad, C. Sun, L. Xing, W. Lin, *J. Am. Chem. Soc*., 2014, **17**, 6171. (c) L. Wang, Y.-A. Li, F. Yang, Q.-K. Liu, J.-P. Ma, Y.-B. Dong, *Inorg. Chem*., 2014, **53**, 9087.
4. (a) M.-H. Zeng, Q.-X. Wang, Y.-X. Tan, S. Hu, H.-X. Zhao, L.-S. Long, M. Kurmoo, *J. Am. Chem. Soc*., 2010, **132**, 2561; (b) A. A. Talin, A. Centrone, M. E. Foster, V. Stavila, P. Haney, R. A. Kinney, V. Szalai, F. El Gabaly, H. P. Yoon, *Science,* 2014, **6616**, 66.
5. (a) J. A. Real, A. B. Gaspar, M. C. Munoz, *Dalton Trans*., 2005, 2062; (b) C. J. Kepert, *Chem. Commun*., 2006, 695; (c) M. Kurmoo, *Chem. Soc. Rev*., 2009, **38**, 1353; (d) A. Bousseksou, G. Molnar, L. Salmon, W. Nicolazzi, *Chem. Soc. Rev*., 2011, **40**, 3313.
6. (a) N. Sabbatini, M. Guardigli, J.-M. Lehn, *Coord. Chem. Rev*., 1993, **123**, 201; (b) A. W. Czarnik, *Acc. Chem. Res*., 1994, **27**, 302; (c) D. Parker, P. K. Senanayake, J. A. G. Williams, *J. Chem. Soc. Perkin Trans*., 1998, **2**, 2129; (d) J. Cui, Z. Lu, Y. Li, Z. Guo, H. Zheng, *Chem. Commun.,* 2012, **48**, 7967; (e) B. Gole, A. K. Bar, P. S. Mukherjee, *Chem. Commun*., 2011, **47**, 12137; (f) S.-R. Zhang, D.-Y. Du, J.-S. Qin, S.-L. Li, W.-W. He, Y.-Q. Lan, Z.-M. Su, *J. Am. Chem. Soc*. 2014, **53**, 8105.
7. (a) W. Liu, T. Jiao, Y. Li, Q. Liu, M. Tan, H. Wang, L. Wang, *J. Am. Chem. Soc.,* 2004, **126**, 2280; (b) B. Zhao, X.-Y. Chen, P. Cheng, D.-Z. Liao, S.-P. Yan, Z.-H. Jiang, *J. Am. Chem. Soc.,* 2004, **126**, 15394; (c) B. Gole, A. K. Bar, P. S. Mukherjee, *Chem. Commun*., 2011, **47**, 12137.

8. M. D. Allendorf, C. A. Bauer, R. K. Bhakta, R. J. T. Houk, *Chem. Soc. Rev.,* 2009, **38**, 1294.
9. (a) J. Rocha, L. D. Carlos, F. A. A. Paz, D. Ananias, *Chem. Soc. Rev*., 2011, **40**, 926; (b) W.-G. Lu, L. Jiang, X.-L. Feng, T.-B. Lu, *Inorg. Chem*., 2010, **48**, 6997; (c) N. Wei, Y.-R. Zhang, Z.-B. Han, *CrystEngComm,* 2013, **15**, 8883.
10. (a) C. J. Kepert, *Chem. Commun*., 2006, 695. (b) G. Férey, *Nat. Mater*., 2003, **2**, 136.
11. (a) N. Masciocchi, S. Galli, V. Colombo, A. Maspero, G. Palmisano, B. Seyyedi, C. Lamberti, S. Bordiga, *J. Am. Chem. Soc.,* 2010, **132**, 7902; (b) Z. B. Han, G. X. Zhang, M. H. Zeng, C. H. Ge, X. H. Zou, G. X. Han, *CrystEngComm,* 2009, **11**, 2629.
12. (a) Z.-B. Han, G.-X. Zhang, M.-H. Zeng, D.-Q. Yuan, Q.-R. Fang, J.-R. Li, J. Ribas, H.-C. Zhou, *Inorg. Chem*., 2010, **49**, 769; (b) Z.-B. Han, J.-W. Ji, H.-Y. An, W. Zhang, G.-X. Han, G.-X. Zhang, L.-G. Yang, *Dalton Trans*., 2009, 9807.
13. G. M. Sheldrick, SHELXTL, Version 6.10, Bruker Analytical X-ray Systems, Madison, WI, USA, 2001.
14. A. L. Spek, *Acta Crystallogr.,* 2009, **D65**, 148.
15. M. D. Allendorf, C. A. Bauer, R. K. Bhakta, R. J. T. Hou, *Chem. Soc. Rev.,* 2009, **38**, 1330.
16. (a) J. Li, C. C. Ji, L. F. Huang, Y. Z. Li, H. G. Zheng, *Inorg. Chem. Acta.,* 2011, **371**, 33; (b) X. Q. Liu, Y. Y. Liu, Y. J. Hao, X. J. Yang, B. Wu, *Inorg. Chem. Commun*., 2010, **13**, 513; (c) E.-C. Yang, J. Li, B. Ding, Q.-Q. Liang, X.-G. Wang and X.-J. Zhao, *CrystEngComm,* 2008, **10**, 158. (d) W.-G. Lu, L. Jiang, X.-L. Long, T.-B. Lu, *Cryst. Growth Des*., 2006, **6(2)**, 564.
17. N. Arnaud, E. Vaquer, J. Georges, *Analyst,* 1998, **123**, 261.
18. (a) Z. Chen, Y. Sun, L Zhang, D. Sun, F. Liu, Q. Meng, R. Wang, D. Sun, *Chem. Commun*., 2013, **49**, 11557; (b) E. Oliveira, C. Nuñez, B. Rodríguez-González, J. L. Capelo, and C. Lodeiro, *Inorg. Chem.,* 2011, **50(18)**, 8797; (c) J. An, C. M. Shade, D. A. Chengelis-Czegan, S. Petoud, N. L. Rosi, *J. Am. Chem. Soc*. 2011, **133**, 1220; (d) M. Zheng, H. Q. Tan, Z. G. Xie, L. G. Zhang, X. B. Jing and Z. C. Sun, *ACS Appl*. *Mater*. *Interfaces*, 2013, **5**, 1078.
19. (a) W. S. Liu, T. Q. Jiao, Y. Z. Li, Q. Z. Liu, M. Y. Tan, H. Wang, L. F. Wang, *J. Am. Chem. Soc*., 2004, **126**, 2280; (b) N. Wei, M.-Y. Zhang, X.-N. Zhang, G.-M. Li, X.-D. Zhang, Z.-B. Han, *Cryst. Growth Des*., 2014, **14(6)**, 3002.
20. M. J. Hossain, M Yamasaki, M. Mikuriya, A. Kuribayashi, H. Sakiyama, *Inorg. Chem*., 2002, **41**, 4058.
21. H. Yang, J. M. Chen, J. J. Sun, S. P. Yang, J. Yu, H. Tan, W. Li, *Dalton Trans*., 2009, 2540.
22. S. Zhang, N.-X. Sun, L. Li, Z-B Han, Y.-Z. Zheng, *Rsc. Adv*., 2014, **4**, 5740.
23. (a) Y. Li, W.-Q. Zou, M.-F. Wu, J.-D. Lin, F.-K. Zheng, Z.-F. Liu, S.-H. Wang, G.-C. Guo, J.-S. Huang, *CrystEngComm,* 2011, **13**, 3868; (b) J. P Zhao, B. W. Hu, Q. Yang, X. F. Zhang, T. L. Hu, X. H. Bu, *Dalton Trans*., 2010, **39**, 56; (c) Z. Shen, J. L. Zuo, Z. Yu, Y. Zhang, J. F. Bai, C. M. Che, H. K. Fun, J. J. Vittal, X. Z. You, *J. Chem. Soc., Dalton Trans*., 1999, 3393; (d) Z.-B. Han, R.-Y. Lu, Y.-F. Liang, Y.-L. Zhou, Q Chen, M.-H. Zeng, *Inorg. Chem*., 2012, **51**, 674; (e) M.-Y. Zhang, W.-J. Shan, Z.-B. Han, *CrystEngComm*, 2012, **14**, 1568.

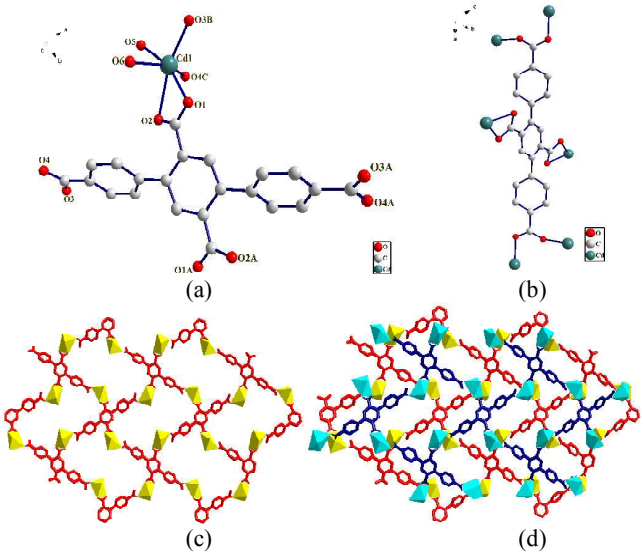

Fig. 1 (a) Coordination environment of Cd(II) center in **1**. Symmetry mode: A: x, y, z. B: 1+x, 1.5-x, 0.5+z. C: x, 1+y, z. (b) The coordination modes of TPTC ligand in **1**. (c) 2D layer structure constructed by Cd(II) and TPTC ligands along the *a*-axis in **1**. (d) The 1D channel of **1** in the 3D framework along the *c*-axis, embedded by the DMA molecules.

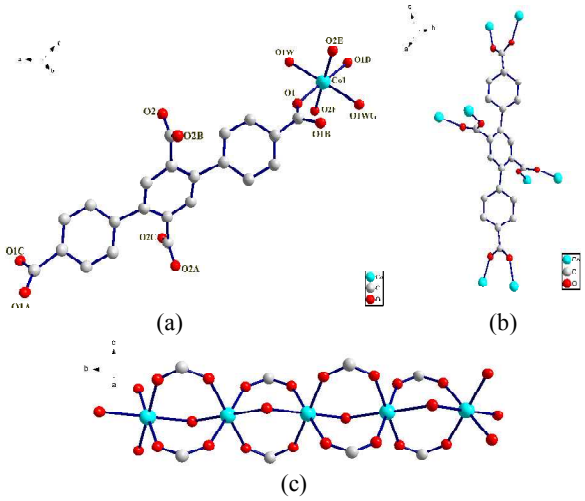

Fig. 2 (a) Coordination environment of Co(II) center in **2**. Symmetry mode: A: x, y, z. B: x, -y, z. C: 0.5-x, 0.5+y, 1-z. D: 0.5-x, 0.5-y, 1-z. E: -0.5+x, 0.5+y, z. F: 1-x, -y,1-z. G:0.5-x, 0.5-y,1-z.. (b) The coordination modes of TPTC ligand in **2**. (c) 1D Co–carboxylate chain along the *b*-axis in **2**.

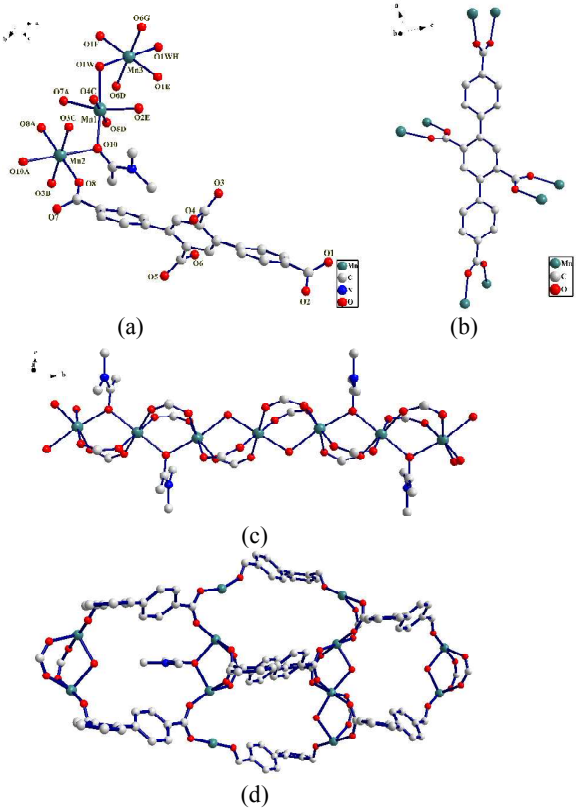

Fig. 3 (a) Coordination environment of Mn(II) center in **3**. Symmetry mode: A: 1-x, 1-y, -z. B: -1+x, y, z. C: 2-x, 1-y, -z. D: 1.5-x, -0.5+y,0.5-z. E: 2.5-x, -0.5+y, 0.5-z. F:-1.5+x, 0.5-y, -0.5+z. G: -0.5+x, 0.5-y, -0.5+z. H: 1-x, -y, -z. (c) The coordination modes of TPTC ligand in **3**. (c) 1D Mn-carboxylate chain along the *b*-axis in **3**. (d) The 1D channel of **3** in the framework along the *a*-axis, embedded by DMA molecules.

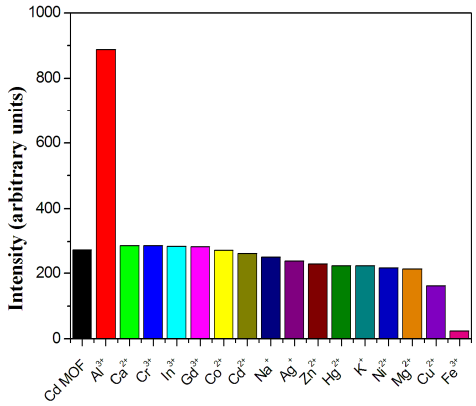

Fig. 4 Room-temperature luminescent intensity of **1** at 390 nm in methanol suspension upon addition of various metal ions (excited at 250 nm).

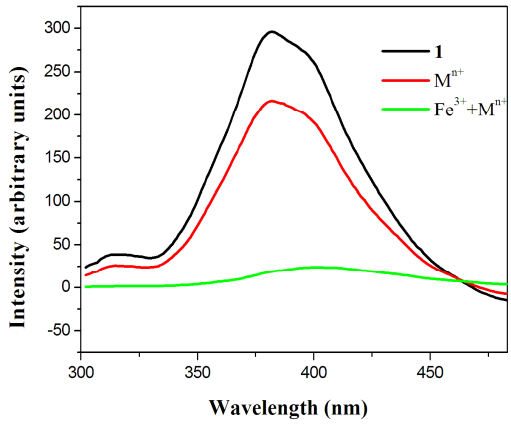

(a)

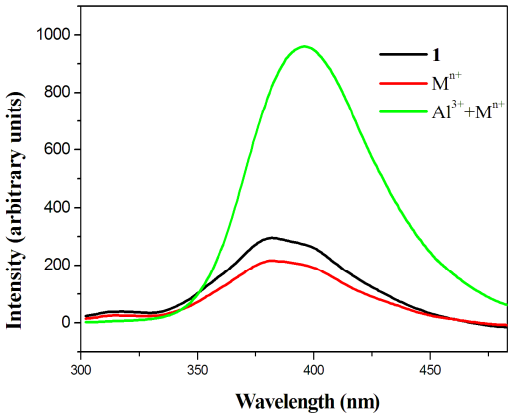

(b)

Fig. 5 Comparison of the photoluminescence intensity of **1** in methanol suspension with the introduction of other M^{n+} ions (Na^{+}, Hg^{2+}, Mg^{2+}, Ni^{2+}, Zn^{2+}) in the absence and presence of 10 equiv Fe^{3+} (a) and 9 equiv Al^{3+} (b).

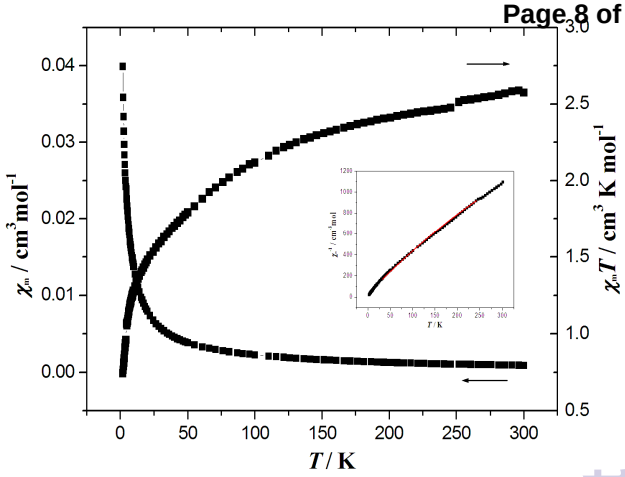

(a)

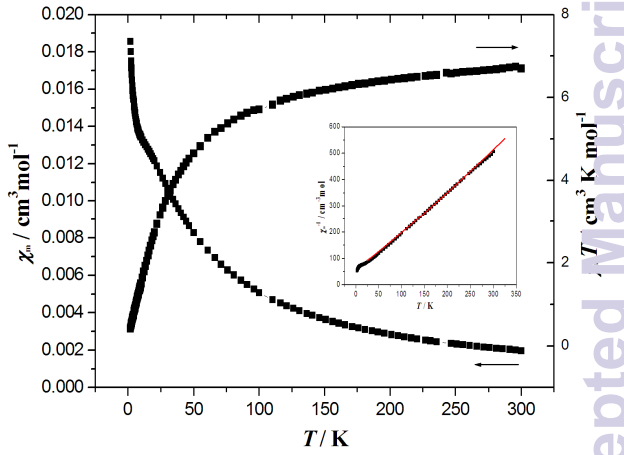

(b)

Fig. 6 Temperature dependence of $\chi_M T$ and χ_M under an applied field of 1 kOe for **2** (a) and **3** (b). The inset shows χ_M^{-1} vs. T plot.